Development of a High-Speed Electrohydraulic Servovalve System Using Stack-Type Piezoelectric Elements

Choon-Shik Joo[1], Young-Bong Bang[1,#], Kyo-Il Lee[1] and Young-Bo Shim[2]

[1] School of Mechanical and Aerospace Engineering, Seoul National University, Seoul, Korea
[2] Samsung Advanced Institute of Technology, Seoul, Korea

ABSTRACT

This paper presents a two-stage electrohydraulic servovalve with a nozzle-flapper pilot stage, which is controlled by stack-type piezoelectric elements. The flapper moving mechanism developed in this research can compensate for the hysteresis problem and thermal expansion of the piezoelectric elements. The experimental result shows that this flapper moving mechanism has the frequency response of about 600 Hz. And a simplified servovalve system using this flapper moving mechanism has the frequency response of about 300 Hz at the supply pressure of 210 bar.

Key Words : servovalve, piezo, flapper, displacement-magnifying mechanism, thermal expansion

Nomenclature

B_s = damping coefficient of main spool
C_{do} = discharge coefficient of supply orifice
C_{df} = discharge coefficient of nozzle
C_{dd} = discharge coefficient of exhaust orifice
D_{si} = inner diameter of main spool
$D_{so} = D$ = outer diameter of main spool
D_o = diameter of supply orifice
D_n = diameter of nozzle
D_d = diameter of exhaust orifice
k_f = stiffness of flow force on spool
M_s = mass of main spool
P_{n1} = pressure of chamber #.1 (left chamber of main spool)
P_{n2} = pressure of chamber #.2 (right chamber of main spool)
P_e = pressure of exhaust chamber
x_v = displacement of main spool
x_f = displacement of flapper

x_{f0} = initial displacement of flapper
V_{n1} = initial volume of chamber #.1
V_{n2} = initial volume of chamber #.2
V_e = initial volume of exhaust chamber
β = bulk modulus of oil
ρ = density of oil
Q_L = load flow
P_s = supply pressure
P_L = load pressure difference
$w = \pi D$

1. Introduction

A servovalve is an intermediate element that connects the hydraulic device with the electric device. Generally, a spool of servovalve moves by an input of low-level electric signal and due to the spool movement, flow or pressure is controlled. A servovalve is used in industrial heavy machine, robot, aerospace engineering and weapon system. Because the performance of a servovalve limits the performance of total system, improving the servovalve performance is significant.

The performance of servovalve depends on many system parameters including the accuracy and tolerance of manufacturing. As it is very difficult to improve the accuracy and tolerance of manufacturing, most of

researches focus on improving the system parameters. Researches done by Lin[1], Martin[2], Ham[3] and Lee[4] study analysis and determination of servovalve parameters. However, other researches about developing a servovalve with new mechanism can be found. Especially, Urai[5], Ohuchi[6] and Yokota[7] apply smart materials to servovalve system. However, these developed servovalves with new mechanism often show poor practicality. Direct-drive type servovalve using smart material developed by Urai and Yokota has no sufficient displacement of spool; thus it is quite difficult to apply it to real application. Servovalve developed by Ohuchi use magnetostrictive material and it needs a high voltage of 600 V to drive magnetostrictive material, moreover this material is exposed to high pressure and high temperature operating oil.

Fig. 1 shows a general two-stage nozzle-flapper type servovalve. The total performance of servovalve is determined by the performance of torque motor in pilot stage and parameters of main valve stage and manufacturing accuracy of valve parts. Even if valve parts are accurately designed and well manufactured, the limitation of performance of torque motor decreases the total servovalve performance. This means that if the performance of flapper moving part is enhanced, total valve performance will be improved.
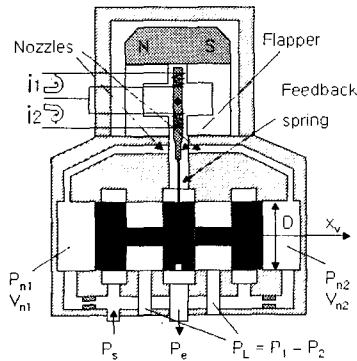

Fig. 1 Two-stage servovalve with nozzle-flapper pilot stage using torque motor

By this concept, this paper shows developed flapper moving mechanism using piezoelectric element and aims to improve servovalve performance by substituting torque motor with developed flapper moving mechanism. Simultaneously, developed servovalve system is designed to satisfy the condition of real application.

2. Simulation of Servovalve System

To design the main part of servovalve, it is necessary to check the dynamic characteristics of servovalve. As mentioned previously, the performance of servovalve changes according to various valve parameters. However, this paper does not target the analysis of valve parameters, valve parameters are determined according to our target specification of servovalve. Then simulation process is performed.

In Fig. 1, the pressure difference between nozzle and flapper occurs by small displacement of flapper in pilot-stage. Since this pressure difference leads to the pressure difference of spool end chambers, it finally drives spool movement. Torque motor drives flapper displacement in case of general two-stage servovalve and the dynamic characteristics of torque motor has to be considered in process of simulation. But our objective is to develop the flapper moving mechanism that has the superior performance to torque motor, so in simulation process, the dynamic performance of flapper is neglected. Likewise, the pressures of spool ends and return chamber are assumed to be constant with respect to time.

Under these assumptions, the valve theories by Merritt[8] are referred and the following governing equations of servovalve are derived.

Equation of motion of spool :

$$\dot{x}_v = \frac{dx_v}{dt}$$

$$\ddot{x}_v = \frac{1}{M_s}\left\{ -B_s\dot{x}_v - k_f x_v + \frac{\pi\left(D_{so}{}^2 - D_{si}{}^2\right)}{4}\left(P_{n1} - P_{n2}\right)\right\} \quad (1)$$

Continuous equation of chamber #.1 :

$$\frac{dP_{n1}}{dt} = \frac{\beta}{V_{n1}}\left\{ C_{do}\left(\frac{\pi D_o{}^2}{4}\right)\sqrt{\frac{2}{\rho}\left(P_s - P_{n1}\right)} - \right.$$

$$\left. C_{df}\pi D_n\left(x_{f0} + x_f\right)\sqrt{\frac{2}{\rho}\left(P_{n1} - P_e\right)} - \frac{\pi\left(D_{so}{}^2 - D_{si}{}^2\right)}{4}\dot{x}_v\right\} \quad (2)$$

Continuous equation of chamber #.2 :

$$\frac{dP_{n2}}{dt} = \frac{\beta}{V_{n2}}\left\{ C_{do}\left(\frac{\pi D_o{}^2}{4}\right)\sqrt{\frac{2}{\rho}\left(P_s - P_{n2}\right)} - \right.$$

$$\left. C_{df}\pi D_n\left(x_{f0} - x_f\right)\sqrt{\frac{2}{\rho}\left(P_{n2} - P_e\right)} + \frac{\pi\left(D_{so}{}^2 - D_{si}{}^2\right)}{4}\dot{x}_v\right\} \quad (3)$$

Continuous equation of return chamber :

$$\frac{dP_e}{dt} = \frac{\beta}{V_e}\left\{ C_{df}\pi D_n \left(x_{f0}+x_f\right)\sqrt{\frac{2}{\rho}\left(P_{n1}-P_e\right)} + \right.$$

$$\left. C_{df}\pi D_n \left(x_{f0}-x_f\right)\sqrt{\frac{2}{\rho}\left(P_{n2}-P_e\right)} - C_{dd}\frac{\pi D_d^{\ 2}}{4}\sqrt{\frac{2}{\rho}P_e} \right\} \quad (4)$$

These equations can be expressed in state equation form.

$$x = \left[x_1\ x_2\ x_3\ x_4\ x_5\right]^T = \left[x_v\ \dot{x}_v\ P_{n1}\ P_{n2}\ P_e\right]^T$$

$$u = x_f$$

$$\dot{x}_1 = x_2$$

$$\dot{x}_2 = \frac{1}{M_s}\left\{ -B_s x_2 - k_f x_1 + \frac{\pi\left(D_{so}^{\ 2}-D_{si}^{\ 2}\right)}{4}\left(x_3-x_4\right)\right\}$$

$$\dot{x}_3 = \frac{\beta}{V_{n1}}\left\{ C_{do}\left(\frac{\pi D_o^{\ 2}}{4}\right)\sqrt{\frac{2}{\rho}\left(P_s-x_3\right)} - \right.$$

$$\left. C_{df}\pi D_n\left(x_{f0}+u\right)\sqrt{\frac{2}{\rho}\left(x_3-x_5\right)} - \frac{\pi\left(D_{so}^{\ 2}-D_{si}^{\ 2}\right)}{4}x_2 \right\}$$

$$\dot{x}_4 = \frac{\beta}{V_{n2}}\left\{ C_{do}\left(\frac{\pi D_o^{\ 2}}{4}\right)\sqrt{\frac{2}{\rho}\left(P_s-x_4\right)} - \right.$$

$$\left. C_{df}\pi D_n\left(x_{f0}-u\right)\sqrt{\frac{2}{\rho}\left(x_4-x_5\right)} + \frac{\pi\left(D_{so}^{\ 2}-D_{si}^{\ 2}\right)}{4}x_2 \right\}$$

$$\dot{x}_5 = \frac{\beta}{V_e}\left\{ C_{df}\pi D_n\left(x_{f0}+u\right)\sqrt{\frac{2}{\rho}\left(x_3-x_5\right)} + \right.$$

$$\left. C_{df}\pi D_n\left(x_{f0}-u\right)\sqrt{\frac{2}{\rho}\left(x_4-x_5\right)} - C_{dd}\frac{\pi D_d^{\ 2}}{4}\sqrt{\frac{2}{\rho}x_5} \right\} \quad (5)$$

The state equation (5) was simulated by simulink in MATLAB, and checked the dynamic characteristics of servovalve.

The critical parameters in designing of servovalve are diameter of spool, stroke of spool, diameter of nozzle and diameter of supply orifice. Among them, flow rate is decided by the diameter of spool and the stroke of spool. To get a sufficient flow rate for the real application, these two parameters have to be decided adequately. If the stroke of spool is too small, feedback control of spool displacement and application to some system become difficult. Therefore, after the spool stroke was determined to approximately some hundreds of micrometers, diameter of spool was determined to give satisfaction with the condition of flow rate.

Our target flow rate is 15 lpm at supply pressure of 210 bar. First, spool stroke was fixed to ±350 μm, and considering leakages, to get a flow rate twice that of target value, spool diameter was calculated by using flow rate equation (6) by Merritt[8]. As a result, the diameter of spool was set to 5 mm.

$$Q_L = C_d w x_v \sqrt{\frac{1}{\rho}\left(P_s - \frac{x_v}{|x_v|}P_L\right)} \quad (6)$$

The diameter of nozzle and supply orifice was designed to be 0.4 mm and 0.3 mm respectively, referring to MOOG valve. From these determined values, simulation of valve performance was done. Generally, when testing the dynamic characteristics of servovalve, input is set to 25 % of rated input value. Then, the frequency when phase delay of 90 ° or amplitude decrease of –3 dB occurs is checked. Consequently, reference input of spool displacement is set to ±87.5 μm which is equivalent to a quarter of full spool stroke of ± 350 μm.

As mentioned in beginning of Chapter 2, this type of servovalve operates by pressure difference between nozzle and flapper, so it is natural that the distance between nozzle and flapper is very sensitive parameter. Hence, the displacement of flapper was assumed to be ± 20 μm, at first, and while changing the displacement between nozzle and flapper, the dynamic characteristics of servovalve was checked. Fig. 2, Fig. 3 and Fig. 4 show the simulation results when displacement between nozzle and flapper is 30 μm, 50 μm and 100 μm, respectively. The points on graphs mean the amplitude decrease or phase delay at each frequency, and the curves are acquired by polynomial curve fitting. As a result, the dynamic bandwidth of servovalve is about 900 Hz, 700 Hz, and 450 Hz, respectively.
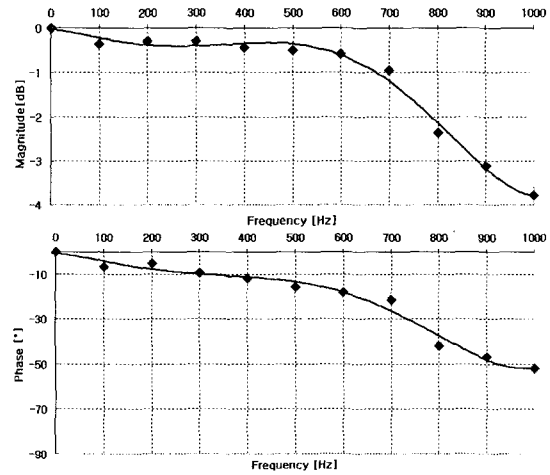
Fig. 2 Simulation of frequency-response characteristics of servovalve when the distance between nozzle and flapper is 30 μm
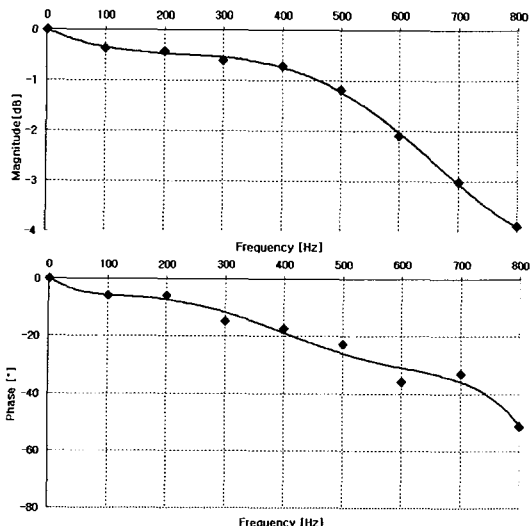
Fig. 3 Simulation of frequency-response characteristics of servovalve when the distance between nozzle and flapper is 50 μm
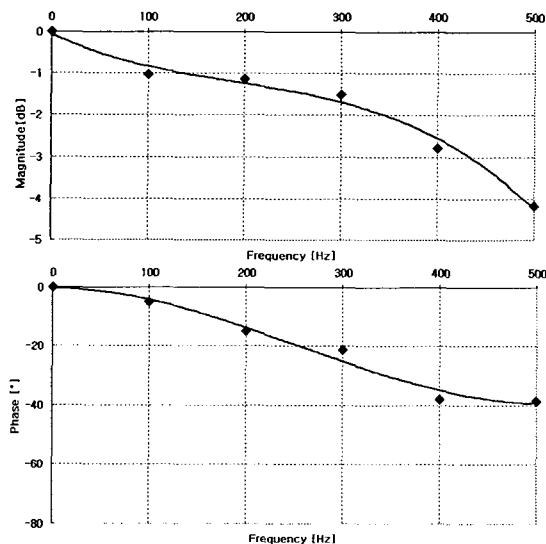

Fig. 4 Simulation of frequency-response characteristics of servovalve when the distance between nozzle and flapper is 100 μm

3. Flapper Moving Mechanism Using Stack-Type Piezoelectric Elements

3.1 Design of Flapper Moving Mechanism

To develop a flapper moving mechanism that performs better than a torque motor, it is necessary to select a new actuator. Stack-type piezoelectric elements were selected among several smart material because of

their large output force and a fast response. The flapper moved by torque motor has over ten micrometers displacements, so the displacement of small stack-type piezoelectric elements is not enough for driving the flapper. Therefore, a new design for displacement-magnifying mechanism is needed.

Table 1 shows the specifications of stack-type piezoelectric elements used in this research. The displacement of a stack-type piezoelectric element becomes half of its full stroke because offset voltage that is half of maximum driving voltage is applied not to drive in negative voltage. Therefore, if the applied offset voltage is 70 V, the possible displacement of piezoelectric elements will be about ±9 μm. Then a structure of displacement magnification is necessary for satisfying the sufficient displacement of flapper.

For designing the displacement-magnifying structure of the piezoelectric element, the hysteretic behavior should be removed while noting that the preload structure is necessary for covering the weakness in tensile force. Moreover thermal expansion should not change the preload or the neutral position of the flapper.

Fig. 5 shows a designed structure that satisfies all of the conditions mentioned previously.

Table 1 Specifications of piezoelectric elements

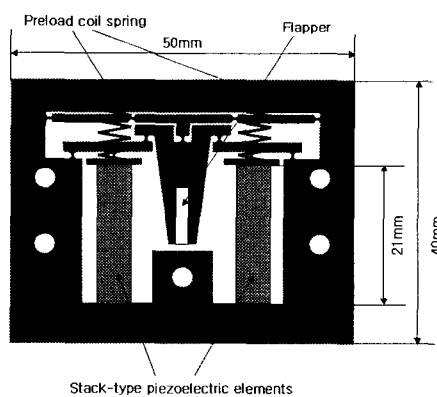| Dimension	21 mm × 4.5 mm × 5.2 mm
Displacement	20 ± 2 μm
Maximum driving voltage	150 V
Capacitance	900 nF ± 20 %
Maximum output force	700 N

Fig. 5 Flapper moving mechanism

As shown in Fig. 5, this is a structure of two-stage displacement magnification using a notch-hinge mechanism. In the first stage, the displacement magnification ratio is 1.78 and in the second stage, it is 2. So the whole displacement magnification ratio is about 3.5, theoretically. The material was chosen to be stainless steel 304. Using the Paros's notch equation (7) in Fig. 6, the maximum deformation of notch was calculated and it was confirmed that there was no problem.
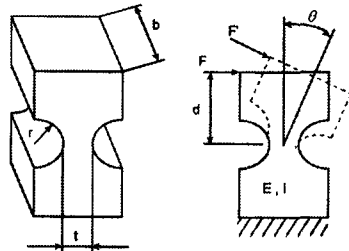

Fig. 6 notch structure

$$\theta_{max} = \frac{4K}{K_t} \frac{R}{Et} \sigma_{max} \left(K_t = \frac{2.7t + 5.4R}{8R + t} + 0.325 \right) \quad (7)$$

Thermal expansion cannot be ignored if maximum strain of the piezoelectric element (about 1/1000) is considered. The upper part of the flapper moving mechanism compensates for the thermal expansion. Increasing two piezoelectric elements by the same length does not affect the flapper position because the hinge structure of the upper part is deformed. That is, because the direction of expansion or contraction of the piezoelectric elements is orthogonal to the direction of flapper movement, the flapper's position is not affected by thermal expansion/contraction of the piezoelectric elements.

Using two piezoelectric elements symmetrically and driving them simultaneously is more effective in reducing hysteretic behavior than using only one element.

Piezoelectric elements are weak in tensile forces, so driving them under a preload condition is recommended. Coil springs apply the preload to piezoelectric element by being compressed into the frame.

3.2 Simulation of Flapper Moving Mechanism

It is hard to expect the theoretical displacement magnification in notch structure because of the elastic deformation in notch, especially in the two-stage

displacement magnification. To measure the loss of the displacement magnification, simulation was performed to confirm the actual displacement magnification and safety of the structure by stress concentration using ANSYS.

Fig. 7 shows the result of simulation when the piezoelectric elements deform by ± 9 μm, which shows the displacement of the flapper is ± 30 μm.

Fig. 8 is the simulation of the maximum stress point and its value. The maximum stress is about 0.2×10^9 Pa. Considering the yielding stress of the stainless steel 304 is 0.883×10^9 Pa, this structure is sufficiently strong with high safety factor close to 4.

Through analyzing the flapper moving mechanism, it can be said that this mechanism has a high safety factor and there is a very little loss in displacement magnification.
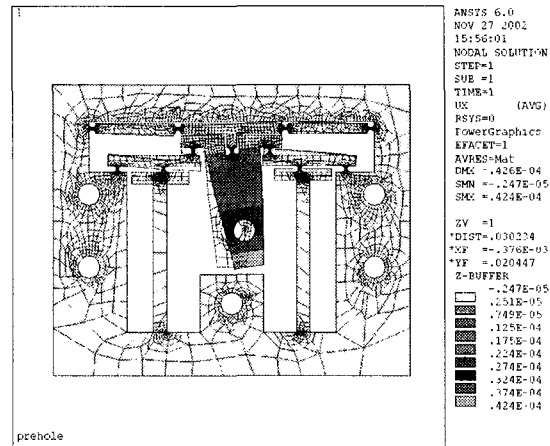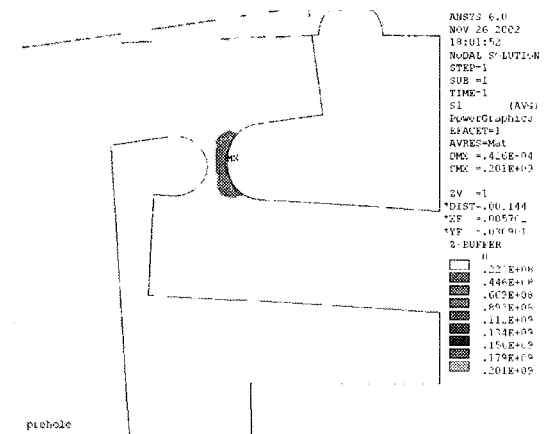

Fig. 7 Simulation of displacement-magnifying mechanism

Fig. 8 Stress concentration of flapper moving mechanism

3.3 Experiment of Flapper Moving Mechanism

The flapper moving mechanism mentioned previously was manufactured and tested to measure the performance in three steps.

The first one measures the flapper deflection and Fig. 9 shows its result. The lead-in wires of the piezoelectric elements were connected in parallel to apply the same voltage to the piezoelectric elements. The input voltage was varied so that the flapper displacement was measured by using an eddy-current-type gap sensor. This experiment indirectly tests flapper deflection caused by the thermal expansion of the piezoelectric elements. As shown in Fig. 9, the flapper deflection was in the range of +1.25 μm ~ −0.5 μm. However, This deflection is negligible because the deflection is not significant compared with the full stroke of the flapper and the deflection does not significantly affect the overall characteristics of the feedback-controlled servovalve system.
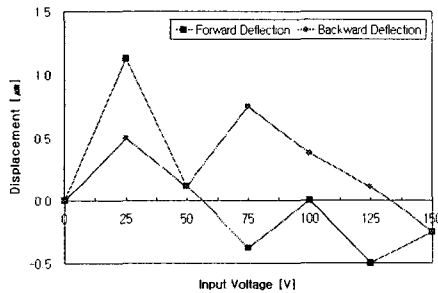

Fig. 9 Flapper deflection versus applied bias voltage

The second one measures the static performance. Fig. 10 illustrates the flapper displacement when the piezoelectric elements are push-pull driven. The bias voltage was 70 V, and the differential driving voltage varied from −70 V to 70 V. As shown in Fig. 10, the displacement of the flapper is about ±25 μm, and nearly proportional to the differential driving voltage. In addition, the hysteretic behavior is quite small.
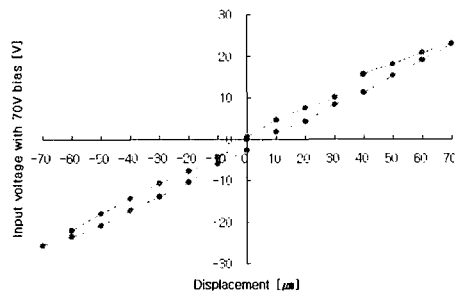

Fig. 10 Static displacement of flapper

The last one checks dynamic characteristics of flapper moving mechanism. Fig. 11 shows the diagram for this experiment. The flapper displacement was measured when two sinusoidal voltages with phase difference of 180 ° were applied to the piezoelectric elements.
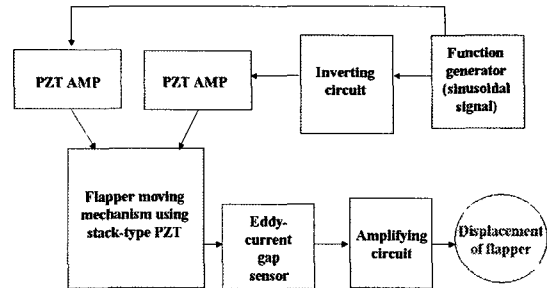

Fig. 11 Experimental setup of flapper moving mechanism

Fig. 12 shows the result of the frequency-response test. The amplitude decrease and the phase delay are within 1.2 dB and 20°, respectively, up to 600 Hz. But the experiment was stopped because there was a resonance at about 600 Hz.
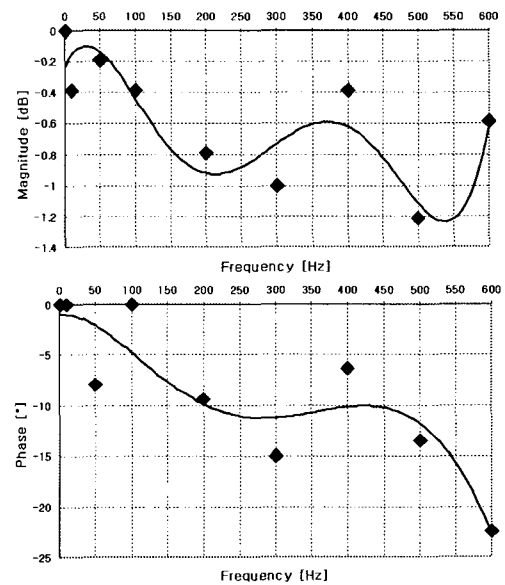

Fig. 12 Frequency-response characteristics of flapper moving mechanism

From the experimental results above, the flapper moving mechanism proposed in this research can compensate for the thermal expansion and the hysteresis problem. Also, the dynamic response is over 600 Hz. The

displacement of the flapper is ±25 μm, which is slightly less than simulation result, that is ±30 μm from the FEA. The output force of the piezoelectric element decreases while the displacement increases, and the output force becomes zero when the displacement is maximized. In case that the piezoelectric element is expanded within the structure, the displacement is reduced because of the reacting force of the notch structure. So it can be said that piezoelectric elements cannot expand up to ±9 μm.

4. Servovalve System

4.1 Design of Simplified Servovalve

The advantages of the designed flapper moving mechanism for servovalve can be confirmed by installing and testing the mechanism on a practical servovalve. For making a practical servovalve, the lands and inlet/outlet ports should be machined extremely accurately, and this accuracy affects the servovalve characteristics. Therefore, by removing inlet/outlet port of the valve, experimental setup and the servovalve design are simplified as shown in Fig. 13. This design has no inlet/outlet port to drive a load, and a coil spring is installed at one end of the spool shaft to compensate the flow force generated from the flow to/from the load. In fact, this type of simplified servovalve is used in developing real servovalves. Because the flow force acting on the spool is proportional to the spool displacement, the simplified servovalve can be used to evaluate the performance of the practical servovalve. This relationship can be modeled by Merritt's equation: the equivalent spring constant of the flow force is described as K_f.

$$K_f = 0.43wP_s \tag{8}$$

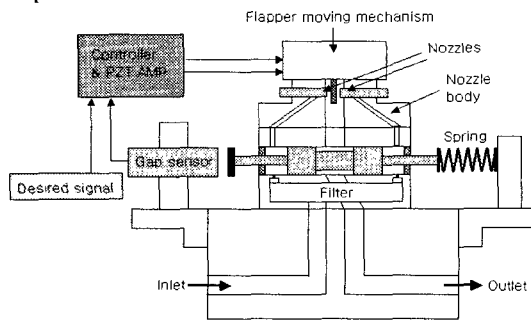The valve dimensions are determined by results of the previous simulation.

Fig. 13 Simplified servovalve system

4.2 Experiment of Servovalve System

Fig. 14 shows the diagram of the control system. Generally, the displacement of a spool is measured by LVDT (Linear Variable Differential Transformer). But, the dynamic characteristics of the LVDT are usually limited to about 500Hz. Thus, an eddy-current gap sensor was used to measure spool displacement. Function generator outputs command signal and error signal between command signal and sensor signal is produced. Output signal from the PD controller is separated into two signals, one of which is the inverted signal of the other one. These two signals are amplified by piezo-amplifiers, and these amplifiers are adjusted to produce the offset voltage E_0, to perform push-pull operation.
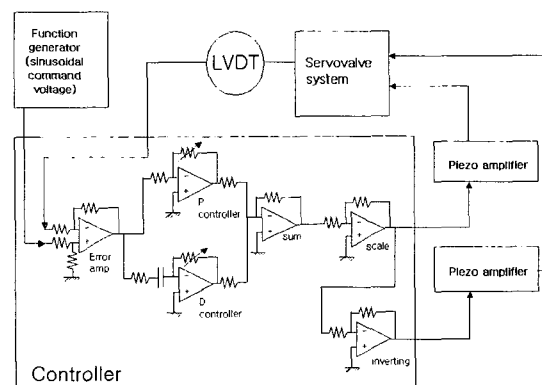

Fig. 14 Servovalve control system

Fig. 15 shows the whole system developed in the research. To evaluate dynamic characteristics of this system, as mentioned in chapter 2, the command signal is set to 25% of rated input value, that is, the amplitude of the command signal is ±87.5 μm which is 1/4 of full stroke of ±350 μm. Fig. 16 shows Bode plot acquired through the experiment raising the frequency from 1 Hz to 500 Hz step by step. This servovalve system shows an amplitude decrease of 3 dB and 90° phase delay at about 300 Hz simultaneously, under the supply pressure of 210 bar. Thus, the bandwidth of this servovalve system is 300 Hz.

From the previous simulation result, the performance of this valve system is extremely sensitive in accordance with a gap between nozzle and flapper. But it is not easy to adjust the gap precisely. In the experiment, the gap between nozzle and flapper was adjusted using microscope, and then the experimental setup was

assembled and tested while readjusting the gap between nozzle and flapper. It is expected that precise gap adjustment will produce an improvement on the result.

Considering the bandwidth of about 100 Hz of general industrial servovalves on market, this paper showed the sufficient possibility of developing high-speed servovalve system with flapper moving mechanism using piezoelectric elements.
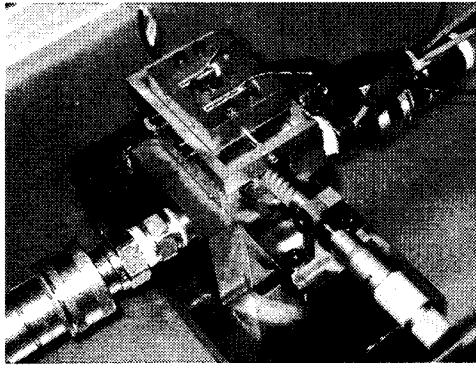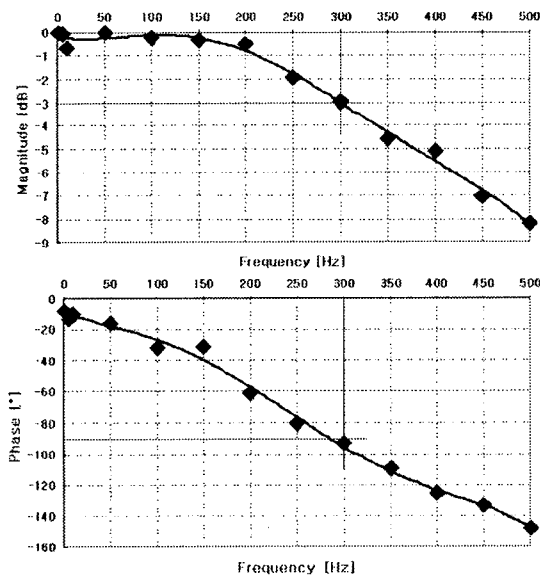

Fig. 15 Experimental setup

Fig. 16 Frequency-response characteristics of simplified servovalve system

5. Conclusions

In this paper, to improve the performance of the two-stage nozzle-flapper type servovalve used in common, the flapper moving mechanism using stack-type

piezoelectric elements is developed. The flapper moving mechanism proposed in this research not only reduces the hysteresis and compensates for the thermal expansion of piezoelectric elements, but also improves the performance of the piezoelectric elements by applying the preload using coil springs and magnifies the displacement of piezoelectric elements by using two-stage notch-hinge structure.

As a result, the flapper moving mechanism has a flapper displacement of ± 25 μm and frequency response of up to 600 Hz. The simplified servovalve system with the flapper moving mechanism was assembled and tested. Under the supply pressure of 210 bar, it has a high dynamic response with a frequency response of about 300 Hz.

Acknowledgement

References

1. Lin, S. J., Akers, A., "A Dynamic Model of the Flapper-Nozzle Component of an Electrohydraulic Servovalve," Journal of Dynamic Systems, Measurement, and Control, Vol. 111, pp. 105-109, 1989.
2. Martin, D. J., Burrows, C. R., "The Dynamic Characteristics of an Electro Hydraulic Servovalve," Journal of Dynamic systems, Measurement, and Control, pp. 395-406, 1976.
3. Ham, Y. B., Yun, S. N., Lee, G. H., Kim, S. D., "A Study on Null Characteristics of 4-way Spool Valve," J. of KSPE, Vol. 12, No. 8, pp. 165-171, 2000.
4. Lee, J. C., "An Analytical Investigation of the Characteristics of Four-Nozzle Flapper Valve," KSPE Spring Annual Meeting, pp. 161-166, 2001.
5. Urai, T., Sugiyama, T., "Development of a direct drive servo valve using a giant magnetostrictive material," Fluid Power, pp. 131-135, 1993.
6. Ohuchi, H., Nakano, K., Uchino, K., Endou, H., Fukumoto, H., Proc. Fluid Control & Measurement, pp. 415, 1985.

7. Yokota, S., Hiramoto, K., Akutsu, K., "An ultra fast-acting electro-hydraulic digital valve and high-speed electro-hydraulic servo valves using multilayered PZT elements," Fluid Power, pp. 121-130, 1993.
8. Merritt, H. E., "HYDRAULIC CONTROL SYSTEMS," New York: John Wiley & Sons, Inc., pp. 6-53, 94, 203, 1967.